Solvent Effect in Dynamic Superstructures from Au Nanoparticles and CdTe Nanowires: Experimental Observation and Theoretical Description

ARTICLE *in* THE JOURNAL OF PHYSICAL CHEMISTRY C · JANUARY 2010

Impact Factor: 4.77 · DOI: 10.1021/jp809780m

4 AUTHORS, INCLUDING:

Jaebeom Lee
Pusan National University
104 PUBLICATIONS **3,255** CITATIONS
SEE PROFILE

Alexander O Govorov
Ohio University
144 PUBLICATIONS **4,755** CITATIONS
SEE PROFILE

Nicholas Kotov
University of Michigan
445 PUBLICATIONS **27,219** CITATIONS
SEE PROFILE

Solvent Effect in Dynamic Superstructures from Au Nanoparticles and CdTe Nanowires: Experimental Observation and Theoretical Description

Jaebeom Lee,*,† Azamat Orazbayev,‡ Alexander O. Govorov,*,‡ and Nicholas A. Kotov*,§

Department of Nanomedical Engineering, College of Nanoscience and Nanotechnology, Pusan National University, Miryang, 627-706, Korea, Department of Physics and Astronomy, Ohio University, Athens, Ohio 45701, and Department of Chemical Engineering, Materials Sciences and Engineering, and Biomedical Engineering, University of Michigan, Ann Arbor, Michigan 48109

Received: November 5, 2008; Revised Manuscript Received: December 9, 2009

Solvent effects on luminescence in nanocolloids are typically related to changes in the dielectric constant around the light-emitting species, but they can have a completely different nature in complex dynamic nanoscale assemblies. Hybrid superstructures were assembled from Au nanoparticles (NPs) and CdTe nanowires (NWs) via poly(ethylene glycol) (PEG) bridges and provide the first example of solvent-responsive dynamic nanoscale assemblies from NWs. The photoluminescence (PL) intensity of the CdTe NWs was found to be dependent on the hydrophilic/hydrophobic balance of the solvent (water, methanol, ethanol, and 2-propanol) surrounding the superstructure and displayed slow equilibration kinetics. PL gradually decreased over a period of 2000 s by ca. 50% for ethanol and ca. 70% for 2-propanol, whereas it remained constant for water and methanol. This phenomenon was attributed to the solvent dependence of the radius of gyration (R_F) of the PEG bridges between the NPs and NWs, which swells in ethanol and 2-propanol. The average distance between the NPs and NWs affects the plasmon−exciton interactions responsible for optical processes in the superstructure, and expansion results in a decrease of the luminescence enhancement of CdTe by Au NPs. Theoretical modeling was carried out to confirm the mechanism of the solvent effect. Exciton−plasmon resonance was described as a combination of two components: field enhancement and energy transfer. Although carrying some limitations and being inherently approximate, this approach was able to describe the distance dependence of the PL intensity of NP−NW system well. The suggested theoretical model expands the understanding of plasmon−exciton electronic systems and can be applied to many semiconductor−metal superstructures.

1. Introduction

There has been considerable interest in the nanomaterial assembly of hybrid superstructures through biological, organic, and polymeric tethers in order to better understand the fundamental physicochemical properties on the nanoscale and tailor materials for novel electronic, sensing, nonlinear optical, and biomedical applications.[1−17] Intensive research has been carried out on superstructures from nanoparticles (NPs).[18−23] These hybrid assemblies of greater complexity than single nanocolloids can be adapted for a variety of novel molecular-engineered applications.[18−23] However, there are only few reports on the combination of zero- and one-dimensional materials in superstructures, exemplified, for instance, by the combination of NPs and carbon nanotubes.[24−28] The introduction of nanowires (NWs) or nanotubes in the superstructures is interesting from the fundamental point of view, but also from the perspective of the utilization of special optical and electronic effects of one-dimensional quantum-confined systems,[29,30] predominantly for sensing and light harvesting. Other fundamentally interesting studies, such as mimicking large biological systems,[31−34] also become possible with such assemblies. All of these applications become possible as long as one can (1) identify the methods of the assembly of NP−NW superstructures and (2) understand how their electronic properties vary with environment. Solvent effects are indispensible for sensing, performing charge-transfer reactions, and understanding their behavior at biointerfaces.

In this study, a nanostructured system was created from NPs and NWs conjugated by poly(ethylene glycol) (PEG) chains. Unlike many other systems made from NPs and one-dimensional nanomaterials, these superstructures are dynamic; that is, they are able to change their structure in response to local conditions. This property originates from the flexible nature of the PEG bridges between the NPs and NWs, which are conformationally responsive to many environmental parameters. As such, the coiling of the PEG linker is affected by interactions with solvents, which results in an increase in the gap between the NPs and NWs in the NP−PEG−NW superstructure for certain solvents. Resonance conditions between the plasmonic and excitonic excitation modes in the superstructures result in changes in the intensity of photoluminescence (PL) in response to the swelling of PEG, thereby providing coupling between the mechanical transitions in the superstructure assembly and its optical properties. The distinction of the time-based PL spectra in various solvents obtained experimentally was also explained theoretically. In addition to confirming the mechanisms of the solvent effect, this part of work also expands the understanding of the nature of exciton−plasmon resonance and related phenomena.

2. Experimental Section

$Cd(ClO_4)_2 \cdot H_2O$, thioglycolic acid (TGA), Al_2Te_3, condensed H_2SO_4, and NaOH were purchased from Aldrich (Milwaukee,

* To whom correspondence should be addressed. E-mail: jaebeom@pusan.ac.kr (J.L.), govorov@helios.phy.ohiou.edu (A.O.G.), kotov@umich.edu (N.A.K.).
† Pusan National University.
‡ Ohio University.
§ University of Michigan.

10.1021/jp809780m
Published on Web 01/06/2010

WI) and used as received. The H_2SO_4 was diluted to 0.5 M with 18 MΩ deionized water (Barnstead E-pure system). This deionized water was used in all experiments. *t*-BOC−NH−PEG−COO−NHS (MW 3400) was purchased from NEKTAR, San Carlos, CA, where NHS and *t*-BOC stand for *N*-hydroxysulfosuccinimide and *tert*-butoxycarbonyl groups, respectively. 1-Ethyl-3-(3-dimethlaminopropyl) carbodiimide hydrochloride (EDC), *N*-hydroxysulfosuccinimide (NHS), and trifluoric acetic acid (TFA) were purchased from Aldrich for conjugation.

The synthesis of CdTe NWs from the NPs is described in detail elsewhere.[29,35] Atomic force microscopy showed the average diameter of CdTe NPs to be 3.7 nm within a 10% standard deviation. The CdTe NWs in water had a diameter, mean length, and PL of 5.8 ± 1.1 nm, 1027 ± 92 nm (giving an aspect ratio of 180), and 644 nm, respectively. The Au NPs were synthesized by Jana et al.'s method using $HAuCl_4$, sodium citrate, and $NaBH_4$.[36] Transmission electron microscopy (TEM; JEOL 2010F) showed NPs that were 3.7 nm in size and had a narrow size distribution.

The stabilizer of Au NPs was then substituted to L-cysteine (Aldrich, Milwaukee, WI) in order to obtain the $-NH_2$ functional group using the following procedures: Two milliliters of Au NPs was mixed with 2−5 mL of acetone and centrifuged at 35000*g* (14000 rpm) for 30 min to separate the Au NPs. The remnant acetone in the separated solution was dried at 60 °C in an oven. The Au NPs were dispersed into an L-cysteine solution (2.5×10^{-7} M) and immersed in an ultrasonic bath for several seconds when aggregates were observed. The L-cysteine-stabilized Au NPs were left to stand at room temperature with gentle stirring for 1 h and then centrifuged before the next step. The approximate molarities of the respective nanomaterials and the molar ratio were calculated; for example, the molarities of the CdTe NWs and Au NPs were ca. 3.99×10^{-9} and 4.51×10^{-6} M, respectively. The molar ratio between the NWs and NPs was approximately 1130:1. The CdTe NWs were diluted four times from the original solution to fit the molarity.

Polymer tethering between the Au NPs and CdTe NWs resulting in NP−PEG−NW was accomplished using two reactive termini, namely, amide groups on the NPs and carboxylic groups on the CdTe NWs. Initially, the functionalized PEG molecules (*t*-BOC−NH−PEG−COO−NHS) were attached to the NH_2 groups of the Au NPs through a reaction with the NHS end. NHS is a good leaving group when there are amide groups. A solution of PEG (10 mg) was prepared in 560 μL of deionized water and 140 μL of dimethyl sulfoxide (DMSO). The L-cysteine-stabilized Au NPs were dispersed into the 700 μL of PEG solution and stirred for 12 h. This caused the tethering of PEG polymers to the Au NP surfaces. A long reaction time and a significant excess of NHS reagent ensured almost complete conversion of all accessible surface amino groups.[37] The *t*-BOC protection of the terminal amine of PEG was removed by adding 1−5 μL of TFA for 20 min. The regenerated $-NH_2$ terminus of PEG was conjugated to the CdTe NWs using standard conjugation techniques, namely, the EDC/sulfo-NHS cross-linking procedure.[38] Fresh solutions of 0.2 M EDC and 25 mM NHS were prepared in a phosphate-buffered saline (PBS) solution (pH 7.2). The solutions of EDC, NHS, and CdTe NWs were mixed at a 1:1:10 ratio with gentle stirring, and the PEG-tethered Au NPs were then added to this solution at a CdTe NW/Au NP volume ratio of 1:1. The solution was stirred gently for 30 min and left to stand for 2 h at room temperature. The surface plasmon of the Au NPs was measured at the end of each experimental step using a UV−vis spectrophotometer (Agilent, model 8453).

The PL of the PEG-tethered Au NP/CdTe NW system was monitored using a time-based fluorescence photometer (Fluoromax-3, Jovin Yvon, Horiba, NJ) with four different solvents, namely, water, methanol, ethanol, and 2-propanol. The prepared sample (10 μL) in the initial solvent was added to a 3-mL cuvette to measure the optical properties. The effect of the small volume of the initial solvent was considered to be negligible. All solvents (spectrophotometric grade or higher, anhydrous) were purchased from Aldrich (Milwaukee, WI) and used without further purification. The PL intensity was monitored every 30−60 s for 30 min at an excitation wavelength of 420 nm and emission wavelengths of 644−666 nm in the respective solvents.

3. Results and Discussion

The UV−vis spectrum of the PEG-coated Au NPs indicates that the surface plasmon absorbance moved slightly to the red and broadened in comparison with that of free NPs (Figure 1a), as a result of the change in the local dielectric environment of the NPs. Broadening of the spectrum is certainly undesirable, but it is probably fairly inevitable because the attachment of PEG increases the diversity of average dielectric constant around the particles and could result in some dynamic aggregates as well, connected by hydrogen bonds through the PEG chains. The flatter broadened peaks also provide more stable plasmon−exciton resonance conditions considering variation of PL spectra of NWs in different solvents (Figure 1b). The red shift of the Au NP absorbance is quite beneficial in our case because it results in stronger spectral overlap with the PL peak of the NWs, which emit at longer wavelengths than the corresponding NPs.

Scanning TEM images of NP−PEG−NWs were obtained to gain insight into the structure of the prepared superstructures (Figure 1c). One can clearly see that the NW is surrounded by a cloud of polymers with imbedded Au NPs, which confirms the expected structure of the NP−PEG−NW assembly. Note that one needs to treat the structure of these assemblies not as something rigid and very well-defined. There is most certainly a great deal of variation in the positioning of the NPs around the NWs at any given moment. To some degree, we cannot really assign a very well-defined structure to this kind of assembly because of its dynamic nature. This feature will probably be a property of many nanoscale assemblies around the temperature(s) of phase transition(s).

The PL of the CdTe NWs was measured in water, methanol, ethanol, and 2-propanol. The emission wavelengths of the NWs red-shifted slightly in more hydrophobic solvents (Figure 1b), which alter the electromagnetic environment around the NWs, resulting in a slight change in the energy band gap.[39] The time-based fluorescence spectra of the free NWs were virtually independent of the hydrophilic−hydrophobic balance of the solvent and demonstrated a slight increase in PL intensity with time (Figure 2a). The same experiment with the NP−PEG−NW superstructure revealed a strong dependence of PL on the solvent (Figure 2b). The PL intensity of the NWs in all solutions stabilized after ca. 30 min within a 20% standard deviation. The high variability of the PL intensity after immersion into a different solvent might come from the following sources: (1) irregular response of the spacer (i.e., PEG polymer in different solvents might induce distance deviations between many Au NPs and a CdTe NW in the NW−NP superstructure, resulting in various luminescence intensities in the NP−PEG−NW) and (2) the uncontrollable aggregation of the NP−PEG−NW superstructures, which will certainly increase the intensity variability due to scattering as the detection time passes. However, the standard deviation of PL was kept steady within

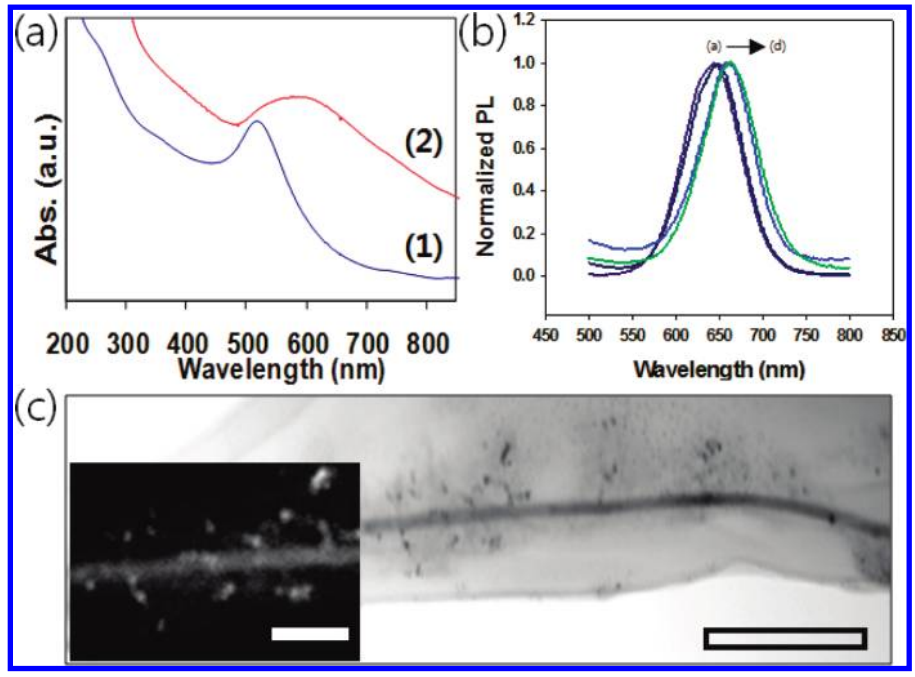

Figure 1. PL spectra of the NWs and TEM images of the NP−PEG−NW superstructures. (a) UV−vis spectra of the Au NPs (1) and PEG-conjugated Au NPs (2). (b) Normalized PL of the CdTe NWs before conjugation in the different solvents: (a) water, (b) methanol, (c) ethanol, and (d) 2-propanol. (c) Scanning TEM images of Au NPs and PEG-tethered CdTe NWs. The scale bar is 200 nm.

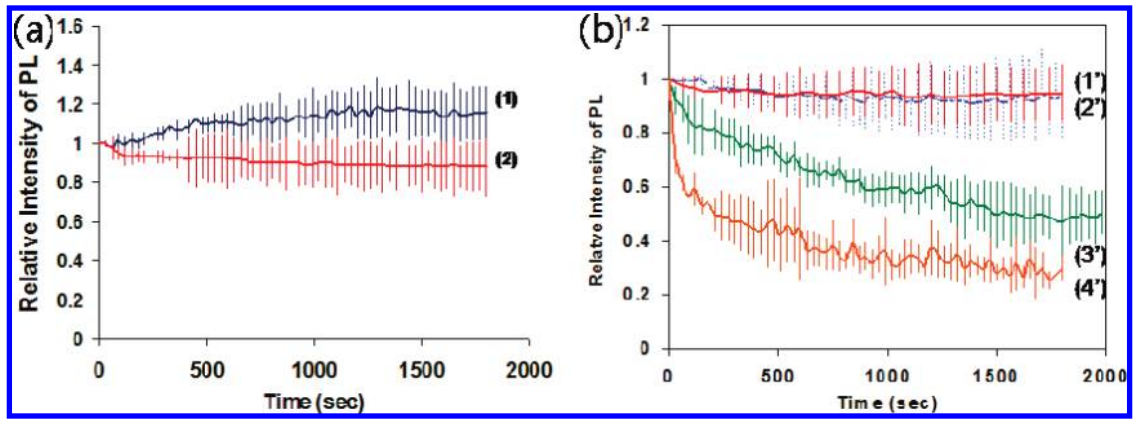

Figure 2. Time-based photoluminescence of NP−PEG−NW in different solvents. (a) NWs without Au NP conjugation: (1) in ethanol and (2) in 2-propanol. (b) NWs with Au NP conjugation: (1′) in water (blue dotted line), (2′) in methanol (red line), (3′) in ethanol, and (4′) in 2-propanol.The vertical lines on each data line show the standard deviations at the respective times.

20% over the whole period of experiments (i.e., 2000 s). This indicates that progressive aggregation was probably not the major source of PL variability, although dynamic aggregation that results in stochastic formation and dissolution of smaller aggregates still needs to be considered.

We were primarily interested in the effect of the solvent on the PL of the NP−PEG−NW superstructure because this system is expected to be quite dynamic as a result of the PEG bridges. The PL kinetics of NP−PEG−NW in water and methanol were similar to each other and to analogous kinetics of NWs without Au−PEG. Overall, they demonstrated almost no change. The luminescence was stable, as expected. No conformational changes were expected in the PEG bridges when an aliquot of the initial aqueous solution was dissolved in water. The hydrophobic−hydrophilic balance of methanol is close to that of water and PEG as well. Importantly, these experiments also demonstrate that there is no change in the intensity of luminescence within the 2000-s time frame due to oxidation with dissolved oxygen.

The PL of the NWs decreased fairly slowly in ethanol, dropping by ca. 50% over the 2000-s period. NP−PEG−NW in 2-propanol showed a rapid decrease in PL intensity, stabilizing at ca. a 70% drop. Within the first 10 min, the drop was around 40%, which correlates very well with the kinetics of PEG swelling in liquid media measured by other researchers.[40] According to their ellipsometric experiments, ca. 40% of the PEG volume swelled within 10 min, whereas less swelling of PEG was observed in water.

The observed solvent effect on PL can be explained by the swelling dynamics of PEG chains in different solvents, causing the average hydrodynamic diameter of PEG (i.e., R_F) to increase.[41−43] The main backbone of PEG can be folded and unfolded by hydrogen-bonding and hydrophobic interactions. Possible conformations of PEG in aqueous solutions can take on a "folded" trans−trans−gauche configuration, in which the oxygen atoms form hydrogen bonds in a variety of ways, leading to a helical supramolecular structure. Therefore, in solvents such as ethanol, PEG expands to form a polymer brush, whereas the PEG polymer chain deswells in water.[37,40,43−47] The conformation of a linearly tethered polymer on a nanomaterial can be a cushion that controls the distance (R_F) between NP and NW in the nanostructure. There are fairly fast components of the

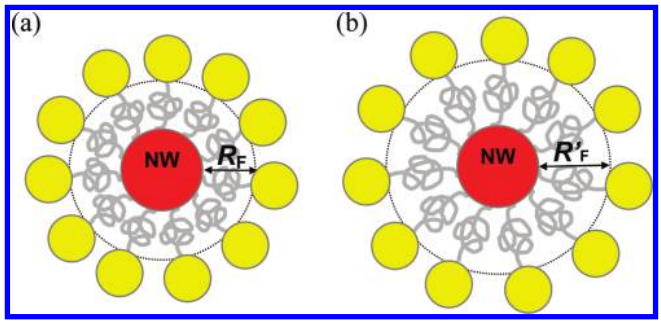

Figure 3. Schematic cross-sectional diagram of the hybrid PEG-tethered NW−NP superstructures in different solvents: (a) in hydrophilic solvents and (b) in hydrophobic solvents. R_F (R'_F) represents the radius of gyration of PEG at the respective solvent conditions. R_F is larger than R'_F. The red circles depict CdTe NWs, and the boundary yellow circles denote the Au NPs. These images are not drawn to scale. Consider also the variability of lengths of PEG chains and, consequently, the gap between the Au NPs and CdTe NW.

process of conformational change in PEG, but the steady-state luminescence is controlled by the slowest process, which is the unfolding of the jammed PEG chains.

Therefore, the mechanism of the solvent effect on PL in NP−PEG−NW can be described as follows: Because there is a strong overlap in the emission spectrum of NWs and the broadened adsorption spectrum of Au NPs (Figure 1a,b), one can expect to see efficient plasmon−exciton resonance similarly to the previously studied NP−PEG−NP superstructures.[9] The resonant conditions result in strong enhancement of the luminescence of CdTe NWs.[9] The intensity of the surface plasmon field coupled to exciton decreases rapidly with increasing distance from the Au NPs.[39,48] Therefore, when the gap between the NPs and NWs increases from R_f in water to R_f' in, say, 2-propanol, it results in a drop in the exciton−plasmon hybridization. Consequently, the PL decreases as well (Figure 3). Therefore, there is a significant drop in the emission in the solvents that cause greater swelling of PEG, such as ethanol and 2-propanol.

This mechanism correlates very well with the experimental data but can also be confirmed by theoretical calculations. For this purpose, we depict the NP−PEG−NW system as an NW with a shell of Au (Figure 4). Considering the schematics in Figures 3 and 4, we must stress again that there will always be considerable spread in distances between Au NPs and CdTe NWs and the suggested description needs to be understood as variations of the average gap between the NPs and NW. The model in Figure 4 also does not incorporate important factors, such as the granularity of the Au shell and the randomness of attached Au NPs. However, the described approximations and simplifications do help when one needs to develop a conceptual description of the mechanism leading to the solvent-sensitive optical responses. The continuous shell model allows for the analytical calculation of the plasmon-induced electromagnetic enhancement inside the NW in the long-wavelength limit, $\lambda \gg R_{shell}$, where λ and R_{shell} are the incident-light wavelength and shell radius, respectively.

To accomplish the theoretical description of electronic effects in NP−PEG−NW,, we suggest using a combination of two well-known processes as the first approximation for exciton−plasmon interactions. The first one is the field enhancement effect generated by plasmons from metal NPs. It describes the concentration of electromagnetic field inside the semiconductor component due the plasmon resonance in the metal NPs. The second one is Förster energy transfer (FRET) describing the

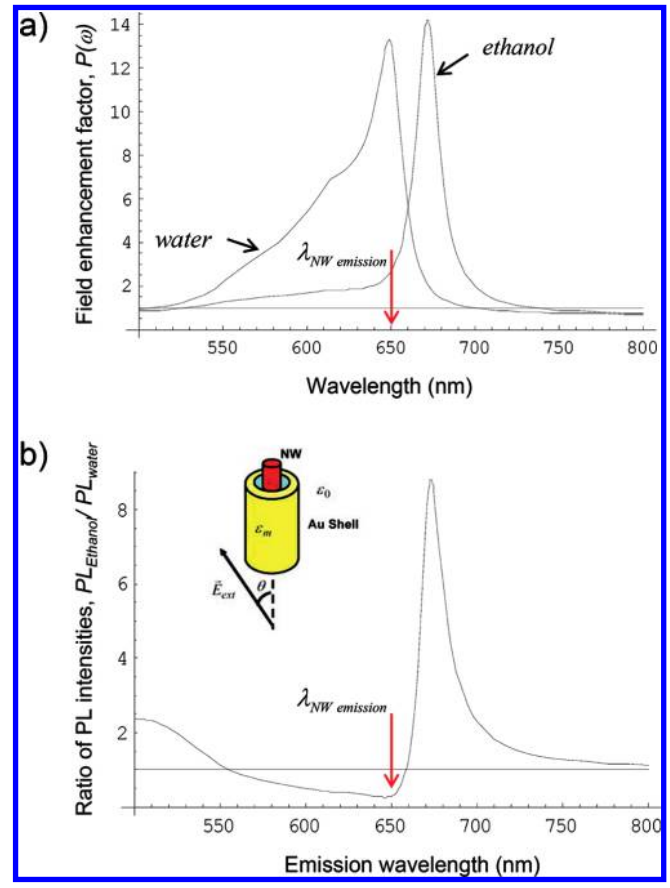

Figure 4. (a) Calculated enhancement factors $P(\lambda)$ for the NW−NP complex in water and ethanol. Internal and external radii of Au shell are given by $R_1 = 2.9$ nm + R_F and $R_2 = 2.9$ nm + R_F + $\Delta_{Au\ shell}$. The NW radius is $R_{NW} = 2.9$ nm; the parameter $\Delta_{Au\ shell}$ is described in the text. (b) Calculated ratio between the PL intensities for ethanol and water [$PL(\lambda_{emiss},R_{F,ethanol})/PL(\lambda_{emiss},R_{F,water})$]. To calculate this ratio, the lengths of PEG in the solvents were taken as $R_{F,water} = 3$ nm and $R_{F,ethanol} = 4.9$ nm; $\lambda_{emiss} = 650$ nm and $\lambda_{abs} = 400$ nm. Inset: Dielectric model of the structure used in calculations.

transfer of excitons from the NWs to the Au NPs. This part of the model depicts the flow of energy from the semiconductor component of the superstructure to the metal component.

The model in Figure 4 has cylindrical symmetry and is described by four dielectric constants: ε_0, $\varepsilon_m(\omega)$, ε_{PEG}, and ε_s. Here, $\varepsilon_0 = 1.8$ is the high-frequency dielectric constant of water (note that, for optical properties, the low-frequency dielectric constant also known as the static dielectric constant equal to 80 is not applicable because of relatively slow kinetics of reorganization of dipolar water molecules); $\varepsilon_m(\omega)$ is the dielectric constant of Au taken from the tables;[49] and $\varepsilon_{PEG} = 2$ and $\varepsilon_s = 7.2$ are the dielectric constants of polymer and CdTe, respectively. In our model, the NW−shell complexes are oriented randomly in a solution, and the incident-light electric field $\vec{E}_{ext}$ forms an arbitrary angle θ with the NW axis (Figure 4, inset). According to the boundary conditions,[50] the field component parallel to the NW ($\vec{E}_{||}$) is not changed inside the dialectic cylinder, whereas the perpendicular component ($\vec{E}_{\perp}$) can be strongly altered, especially in the vicinity of plasmon resonance. The perpendicular component of the total electric field inside the NW is obtained from the boundary conditions and Poisson equation as

$$E_{\mathrm{tot},\perp}/E_{\mathrm{ext},\perp} = -8R_1^2R_2^2\gamma_m\gamma_{PEG}/\{-R_2^2R_W^2(1+\gamma_m)\times(\gamma_m-\gamma_{PEG})(\gamma_{PEG}-\gamma_W)+R_1^4(-1+\gamma_m)(\gamma_m-\gamma_{PEG})\times(\gamma_{PEG}+\gamma_W)-R_1^2(\gamma_m+\gamma_{PEG})[-R_W^2(-1+\gamma_m)\times(\gamma_{PEG}-\gamma_W)+R_2^2(1+\gamma_m)(\gamma_{PEG}+\gamma_W)]\}$$

where $E_{\mathrm{ext(tot)},\perp}$ represents the perpendicular component of the external (total) fields inside the NW; R_W is the NW radius; and R_1 and R_2 are the radii of the internal and external surfaces, respectively, of the Au shell (see the inset in Figure 4 and the figure caption), which are related to R_f and the diameter of the NPs but, strictly speaking, are not exactly equal to them because of differences in the models in Figures 3 and 4. Also, $\gamma_m = \varepsilon_m/\varepsilon_0$, $\gamma_{PEG} = \varepsilon_{PEG}/\varepsilon_0$, and $\gamma_s = \varepsilon_s/\varepsilon_0$. For the parallel components, $E_{\mathrm{tot},||} = E_{\mathrm{ext},||}$. The net enhancement factor for the fields inside the NW, which is the cumulative measure of exciton−plasmon interaction responsible for PL changes, should be found by averaging over all angles θ

$$P(\omega) = \frac{\langle E_{\mathrm{tot}}E_{\mathrm{tot}}^*\rangle_\theta}{E_{\mathrm{ext}}^2} = \frac{(E_{\mathrm{tot},\perp}E_{\mathrm{tot},\perp}^*)/E_{\mathrm{ext},\perp}^2+2}{3}$$

As mentioned above, FRET of excitons to the metal NPs is another important component that will help describe exciton−plasmon interactions in the system, which influences the PL response. To estimate the energy-transfer rate, we now assume that a localized exciton for an NW is transferred to several Au NPs. The rate for transfer to one Au NP can be estimated using the standard FRET theory applied to a semiconductor−metal donor−acceptor pair

$$\gamma_{1,\mathrm{transfer}}(\omega_{\mathrm{exc},d}) \approx \frac{4}{\hbar}\frac{e^2d_{\mathrm{exc}}^2}{d^6\varepsilon_{\mathrm{eff}}^2}R_{\mathrm{NP}}^3\frac{3\varepsilon_0^2\,\mathrm{Im}\,\varepsilon_m(\omega_{\mathrm{exc}})}{|\varepsilon_m(\omega_{\mathrm{exc}})+2\varepsilon_0|^2}$$

where R_{NP} is the Au NP radius, $\varepsilon_{\mathrm{eff}} = (2\varepsilon_0+\varepsilon_s)/3$, ω_{exc} is the NW-exciton frequency, d is a distance between the centers of NW and NP, and $d_{\mathrm{exc}} \approx 0.1$ nm is the typical exciton dipole in a colloidal nanocrystal (for more details, see ref 44). From this expression, we obtain the following estimate for the FRET rate to one Au NP: $\gamma_{1,\mathrm{transfer}} \approx 1/(23\ \mathrm{ns})$. To obtain this number, we have assumed that $d = R_W + R_F + R_{NP}$, $R_F = 3$ nm, and $R_{NP} = 1.75$ nm. In the next step, we should notice that an exciton can be transferred to several neighboring Au NPs. If we now include transfer to all neighboring Au NPs from an exciton located in the center of the NW (see Figure 3a), the total rate of transfer becomes $\gamma_{\mathrm{trasfer}} \approx 1/(1.3\ \mathrm{ns})$.[51] Time-resolved PL study of isolated nanowires provided a relatively short exciton lifetime, $\tau_0 \approx 1$ ns. In addition, the quantum yield of our NWs is about 1% ($Y = 0.01$), which gives a radiative lifetime of $\tau_{\mathrm{rad}} \approx 100$ ns. Now, we can see that Förster transfer is an important process because $\gamma_{\mathrm{transfer}} \approx \gamma_0 = 1/\tau_0$. In particular, the exciton lifetime of NW−PEG−NP superstructure becomes essentially shortened to $\tau_{\mathrm{NW-NP}} = 1/(\gamma_{\mathrm{trasfer}}+\gamma_0) < 1/\gamma_0$. This shortening of lifetime has been observed, for example, in ref 2.

Now, we need to combine the field enhancement and the FRET process as two energy flow components contributing to the solvent dependence of PL in Figure 2. We can conclude that (a) the electromagnetic field intensity in the NW depends on R_F, and this solvent effect should be described by a factor $P(\omega)$, and (b) FRET from a CdTe NW to Au NPs depends on R_F, and therefore, the PL intensity of NW becomes sensitive to the distance R_F. As expected, these two mechanisms work against each other, and according to the experimental data in Figure 2, mechanism a wins. Now, we investigate whether we can reproduce this effect mathematically. The PL intensity of a semiconductor emitter is given by

$$\mathrm{PL}(\lambda_{\mathrm{emiss}}, R_F) \propto \gamma_{\mathrm{rad}}^0\frac{P(\lambda_{\mathrm{abs}})\,P(\lambda_{\mathrm{emiss}})}{\gamma_0(1-Y)+\gamma_{\mathrm{rad}}^0P(\lambda_{\mathrm{emiss}})+\gamma_{\mathrm{transfer}}P(\lambda_{\mathrm{emiss}})}$$

where $\gamma_{\mathrm{rad}}^0 = 1/\tau_{\mathrm{rad}}$ is the radiative rate of isolated NWs and $\gamma_0 \gg 1/\tau_{\mathrm{rad}} = Y\gamma_0$.[44] The important electromagnetic factors $P(\lambda_{\mathrm{abs}})$ and $P(\lambda_{\mathrm{emiss}})$ describe the plasmon-induced enhancement for the emission and absorption processes, respectively, and the parameter $\gamma_{\mathrm{transfer}}(\lambda_{\mathrm{emiss}})$ describes the NW−NP energy transfer.[52] Now, we examine what happens to the PL intensity as the PEG expands. For this purpose, we plot the function $\mathrm{PL}(\lambda_{\mathrm{emiss}},R_F)$ for two different R_F values corresponding to the diameters of water and ethanol ($R_{F,\mathrm{water}} = 3$ nm and $R_{F,\mathrm{ethanol}} = 4.9$ nm) (Figure 4a). For the thickness of the continuous Au shell, we take $\Delta_{\mathrm{Au\ shell}} = R_2 - R_1 = 3.25$ nm (2.9 nm) in water (ethanol). We have chosen these thicknesses to conserve the total volume of gold in the shell as the shell expands. We see in Figure 4a that both the position and amplitude of the plasmon peak strongly depend on R_F, as does the plasmon enhancement of photon emission. This happens because electric fields associated with the plasmon are very sensitive to the geometry and size of a nanostructure; indeed, multiple literature reports indicate a plasmon dependence on the properties of the medium in close vicinity to the metal surface. From the results shown in Figure 4a, we conclude that the plasmon enhancement strongly depends on the shell radii,[2,9,44,52−54] which provides a mechanism for solvent dependence. We also note that the Au nanoshell is able to create significant electric-field enhancement inside a NW through a strong collective plasmon resonance, as observed in ref 15. An important development of this article, in comparison with ref 15, is in the ability to control the NP−NW distance through the introduction of different solvents. The chemically induced distance variations in our superstructures are recorded optically, as changes in the PL intensity.

For the FRET process, we obtained the estimates $\gamma_{\mathrm{transfer}} \approx 1/(1.3\ \mathrm{ns})$ and $1/(3.9\ \mathrm{ns})$, taking into account that $R_F = 3$ and 4.9 nm. In other words, FRET becomes less efficient for the case of ethanol, as expected. The ratio of PL intensities for the NP−PEG−NW superstructure in water and ethanol is obtained as $\mathrm{PL}(\lambda_{\mathrm{emiss}},R_{F,\mathrm{ethanol}})/\mathrm{PL}(\lambda_{\mathrm{emiss}},R_{F,\mathrm{water}}) \approx 0.3$ for NWs with emission at $\lambda_{\mathrm{NW\ emiss}} = 650$ nm (Figure 4b). The PL intensity in ethanol is weaker because the plasmon enhancement is strongly reduced because of a longer R_F. The corresponding experimental ratio is ~0.5 (Figure 2). The theory thus qualitatively reproduces the experiment. In conclusion to this discussion of theory, we again emphasize that our calculations should be taken as an appropriate but certainly not complete description of the actual complexity of plasmon−exciton interactions. Nevertheless, the qualitative understanding coming from our model is very helpful and can be used as a guide to synthetic chemists for the design of the nanoscale assemblies. Also, the description of exciton−plasmon interactions in the form of the two components described above can be applied to a variety of nanoscale systems and can certainly be useful as an intermediate

point for further theoretical understanding of the phenomena related to superstructures composed from metal and semiconductor NPs.

4. Conclusions

A strong solvent effect was observed for the PL of NP−PEG−NWs that has a completely different nature than other solvent effects observed for individual nanocolloids. The PL of the NP−PEG−NW superstructures was found to decrease in ethanol and 2-propanol while remaining the same for water and methanol. This can be explained by the swelling of PEG bridges in different solvents, which affects the distance between the NPs and NWs. This effect, in turn, leads to a great change in the intensity of plasmon−exciton interaction. A theoretical model based on the description of exciton−plasmon interactions as two components, namely, field enhancement from the Au NPs in the CdTe NW and FRET from the CdTe NWs to the Au NPs, was used to explain the origin of the PL changes. The plasmon resonance and plasmon-enhanced PL were found to be quite sensitive to any nanomechanical movement/deformation in the system. The theoretical model presented can be used for a variety of superstructures made from metal and semiconductor NPs.

Acknowledgment. This work was supported by a Korea Research Foundation Grant funded by the Korean Government (MOEHRD, Basic Research Promotion Fund) (KRF-2007-331-C00140). A.O.G. and N.A.K. acknowledge financial support from NSF and AFOSR.

References and Notes

(1) Gandhi, D. D.; Lane, M.; Zhou, Y.; Singh, A. P.; Nayak, S.; Tisch, U.; Eizenberg, M.; Ramanath, G. Annealing-induced interfacial toughening using a molecular nanolayer. *Nature* **2007**, *447* (7142), 299–302.

(2) Lee, J.; Hernandez, P.; Lee, J.; Govorov, A. O.; Kotov, N. A. Exciton−plasmon interactions in molecular spring assemblies of nanowires and wavelength-based protein detection. *Nat. Mater.* **2007**, *6* (4), 291–295.

(3) Roy, D.; Fendler, J. Reflection and absorption techniques for optical characterization of chemically assembled nanomaterials. *Adv. Mater.* **2004**, *16* (6), 479–508.

(4) Ishii, T.; Otsuka, H.; Kataoka, K.; Nagasaki, Y. Preparation of Functionally PEGylated Gold Nanoparticles with Narrow Distribution through Autoreduction of Auric Cation by α-Biotinyl-PEG-*block*-[poly(2-(*N*,*N*-dimethylamino)ethyl methacrylate)]. *Langmuir* **2003**, *20* (3), 561–564.

(5) Willner, I.; Willner, B. Functional nanoparticle architectures for sensoric, optoelectronic, and bioelectronic applications. *Pure Appl. Chem.* **2002**, *74* (9), 1773–1783.

(6) Katz, E.; Willner, I. Integrated Nanoparticle.Biomolecule Hybrid Systems: Synthesis, Properties, and Applications. *Angew. Chem., Int. Ed.* **2004**, *43* (45), 6042–6108.

(7) Bauer, L. A.; Birenbaum, N. S.; Meyer, G. J. Biological applications of high aspect ratio nanoparticles. *J. Mater. Chem.* **2004**, *14* (4), 517–526.

(8) West, J. L.; Halas, N. J. Engineered Nanomaterials for Biophotonics Applications: Improving Sensing, Imaging, and Therapeutics. *Annu. Rev. Biomed. Eng.* **2003**, *5* (1), 285–292.

(9) Lee, J.; Govorov, A. O.; Kotov, N. A. Nanoparticle Assemblies with Molecular Springs: A Nanoscale Thermometer. *Angew. Chem.* **2005**, *117* (45), 7605–7608.

(10) Mao, C.; Solis, D. J.; Reiss, B. D.; Kottmann, S. T.; Sweeney, R. Y.; Hayhurst, A.; Georgiou, G.; Iverson, B.; Belcher, A. M. Virus-Based Toolkit for the Directed Synthesis of Magnetic and Semiconducting Nanowires. *Science* **2004**, *303* (5655), 213–217.

(11) Beek, W. J. E.; Wienk, M. M.; Janssen, R. A. J. Efficient Hybrid Solar Cells from Zinc Oxide Nanoparticles and a Conjugated Polymer. *Adv. Mater.* **2004**, *16* (12), 1009–1013.

(12) Pagba, C.; Zordan, G.; Galoppini, E.; Piatnitski, E. L.; Hore, S.; Deshayes, K.; Piotrowiak, P. Hybrid Photoactive Assemblies: Electron Injection from Host-Guest Complexes into Semiconductor Nanoparticles. *J. Am. Chem. Soc.* **2004**, *126* (32), 9888–9889.

(13) Tian, S.; Liu, J.; Zhu, T.; Knoll, W. Polyaniline/Gold Nanoparticle Multilayer Films: Assembly, Properties, and Biological Applications. *Chem. Mater.* **2004**, *16* (21), 4103–4108.

(14) Du, J.; Chen, Y. Organic−inorganic hybrid nanoparticles with a complex hollow structure. *Angew. Chem.* **2004**, *43* (38), 5084–5087.

(15) Lee, J.; Govorov, A. O.; Dulka, J.; Kotov, N. A. Bioconjugates of CdTe Nanowires and Au Nanoparticles: Plasmon−Exciton Interactions, Luminescence Enhancement, and Collective Effects. *Nano Lett.* **2004**, *4* (12), 2323–2330.

(16) Bhat, R. R.; Genzer, J.; Chaney, B. N.; Sugg, H. W.; Liebmann-Vinson, A,. Controlling the assembly of nanoparticles using surface grafted molecular and macromolecular gradients. *Nanotechnology* **2003**, *14* (10), 1145–1152.

(17) Gudiksen, M. S.; Lauhon, L. J.; Wang, J.; Smith, D. C.; Lieber, C. M. Growth of nanowire superlattice structures for nanoscale photonics and electronics. *Nature* **2002**, *415* (6872), 617–620.

(18) Jin, R.; Wu, G.; Li, Z.; Mirkin, C. A.; Schatz, G. C. What Controls the Melting Properties of DNA-Linked Gold Nanoparticle Assemblies. *J. Am. Chem. Soc.* **2003**, *125* (6), 1643–1654.

(19) Parak, W. J.; Pellegrino, T.; Micheel, C. M.; Gerion, D.; Williams, S. C.; Alivisatos, A. P. Conformation of Oligonucleotides Attached to Gold Nanocrystals Probed by Gel Electrophoresis. *Nano Lett.* **2002**, *3* (1), 33–36.

(20) Storhoff, J. J.; Elghanian, R.; Mirkin, C. A.; Letsinger, R. L. Sequence-Dependent Stability of DNA-Modified Gold Nanoparticles. *Langmuir* **2002**, *18* (17), 6666–6670.

(21) Nam, J. M.; Stoeva, S. I.; Mirkin, C. A. Bio-Bar-Code-Based DNA Detection with PCR-like Sensitivity. *J. Am. Chem. Soc.* **2004**, *126* (19), 5932–5933.

(22) Kramer, S.; Xie, H.; Gaff, J.; Williamson, J. R.; Tkachenko, A. G.; Nouri, N.; Feldheim, D. A.; Feldheim, D. L. Preparation of Protein Gradients through the Controlled Deposition of Protein−Nanoparticle Conjugates onto Functionalized Surfaces. *J. Am. Chem. Soc.* **2004**, *126* (17), 5388–5395.

(23) Harnack, O.; Ford, W. E.; Yasuda, A.; Wessels, J. M. Tris(hydroxymethyl)phosphine-Capped Gold Particles Templated by DNA as Nanowire Precursors. *Nano Lett.* **2002**, *2* (9), 919–923.

(24) Carrillo, A.; Swartz, J. A.; Gamba, J. M.; Kane, R. S.; Chakrapani, N.; Wei, B.; Ajayan, P. M. Noncovalent Functionalization of Graphite and Carbon Nanotubes with Polymer Multilayers and Gold Nanoparticles. *Nano Lett.* **2003**, *3* (10), 1437–1440.

(25) Ravindran, S.; Bozhilov, K. N.; Ozkan, C. S. Self assembly of ordered artificial solids of semiconducting ZnS capped CdSe nanoparticles at carbon nanotube ends. *Carbon* **2004**, *42* (8−9), 1537–1542.

(26) Liu, L.; Wang, T.; Li, J.; Guo, Z. X.; Dai, L.; Zhang, D.; Zhu, D. Self-assembly of gold nanoparticles to carbon nanotubes using a thiol-terminated pyrene as interlinker. *Chem. Phys. Lett.* **2003**, *367* (5−6), 747–752.

(27) Larciprete, R.; Lizzit, S.; Botti, S.; Cepek, C.; Goldoni, A. Structural reorganization of carbon nanoparticles into single-wall nanotubes. *Phys. Rev. B* **2002**, *66* (12), 121402−1121402−4.

(28) Homma, Y.; Yamashita, T.; Kobayashi, Y.; Ogino, T. Interconnection of nanostructures using carbon nanotubes. *Physica B: Condensed Matter* **2002**, *323* (1−4), 122–123.

(29) Tang, Z.; Kotov, N. A.; Giersig, M. Spontaneous Organization of Single CdTe Nanoparticles into Luminescent Nanowires. *Science* **2002**, *297* (5579), 237–240.

(30) Lee, J.; Javed, T.; Skeini, T.; Govorov, A. O.; Bryant, G. W.; Kotov, N. A. Bioconjugated Ag Nanoparticles and CdTe Nanowires: Metamaterials with Field-Enhanced Light Absorption. *Angew. Chem.* **2006**, *118* (29), 4937–4941.

(31) Tan, S.; Tang, Z.; Liang, X.; Kotov, N. A. Resonance Tunneling Diode Structures on CdTe Nanowires Made by Conductive AFM. *Nano Lett.* **2004**, *4* (9), 1637–1641.

(32) Lee, J.; Govorov, A. O.; Kotov, N. A. Bioconjugated Superstructures of CdTe Nanowires and Nanoparticles: Multistep Cascade Forster Resonance Energy Transfer and Energy Channeling. *Nano Lett.* **2005**, *5* (10), 2063–2069.

(33) Liang, X.; Tan, S.; Tang, Z.; Kotov, N. A. Investigation of Transversal Conductance in Semiconductor CdTe Nanowires with and without a Coaxial Silica Shell. *Langmuir* **2004**, *20* (4), 1016–1020.

(34) Wang, Y.; Tang, Z.; Liang, X.; Liz-Marzan, L. M.; Kotov, N. A. SiO_2-Coated CdTe Nanowires: Bristled Nano Centipedes. *Nano Lett.* **2004**, *4* (2), 225–231.

(35) Gaponik, N.; Talapin, D. V.; Rogach, A. L.; Hoppe, K.; Shevchenko, E. V.; Kornowski, A.; Eychmuller, A.; Weller, H. Thiol-Capping of CdTe Nanocrystals: An Alternative to Organometallic Synthetic Routes. *J. Phys. Chem. B* **2002**, *106* (29), 7177–7185.

(36) Jana, N. R.; Gearheart, L.; Murphy, C. J. Seeding Growth for Size Control of 5−40 nm Diameter Gold Nanoparticles. *Langmuir* **2001**, *17* (22), 6782–6786.

(37) Westenhoff, S.; Kotov, N. A. Quantum Dot on a Rope. *J. Am. Chem. Soc.* **2002**, *124* (11), 2448–2449.

(38) Hermanson, G. T. *Bioconjugate Techniques*; Academic Press: New York, 1996.

(39) Kreibig, U.; Vollmer, M. *Optical Properties of Metal Clusters*; Springer: Berlin, 1995.

(40) Munro, J. C.; Frank, C. W. Adsorption of Lipid-Functionalized Poly(ethylene glycol) to Gold Surfaces as a Cushion for Polymer-Supported Lipid Bilayers. *Langmuir* **2004**, *20* (8), 3339–3349.

(41) Branca, C.; Faraone, A.; Magazu, S.; Maisano, G.; Migliardo, P.; Villari, V. Swelling processes in aqueous polymer solutions by PCS and Raman scattering. *J. Mol. Struct.* **1999**, *482−483*, 503–507.

(42) Govorov, A. O.; Bryant, G. W.; Zhang, W.; Skeini, T.; Lee, J.; Kotov, N. A.; Slocik, J. M.; Naik, R. R. Exciton−Plasmon Interaction and Hybrid Excitons in Semiconductor-Metal Nanoparticle Assemblies. *Nano Lett.* **2006**, *6* (5), 984–994.

(43) Branca, C.; Magaz'u, S; Maisano, G.; Migliardo, P.; Villari, V *J. Phys.: Condensed Matter* **1998**, *10* (45), 10141–10157, Conformational distribution of poly(ethylene oxide) in molten phase and in aqueous solution by quasi-elastic and inelastic light scattering.

(44) Govorov, A. O.; Carmeli, I. Hybrid Structures Composed of Photosynthetic System and Metal Nanoparticles: Plasmon Enhancement Effect. *Nano Lett.* **2007**, *7* (3), 620–625.

(45) Kaper, H. J.; Busscher, H. J.; Norde, W. Characterization of poly(ethylene oxide) brushes on glass surfaces and adhesion of Staphylococcus epidermidis. *J. Biomater. Sci., Polym. Ed.* **2003**, *14* (4), 313–324.

(46) Huddleston, J. G.; Looney, T. K.; Broker, G. A.; Griffin, S. T.; Spear, S. K.; Rogers, R. D. Comparative Behavior of Poly(ethylene glycol) Hydrogels and Poly(ethylene glycol) Aqueous Biphasic Systems. *Ind. Eng. Chem. Res.* **2003**, *42* (24), 6088–6095.

(47) Savas, H.; Guven, O. Investigation of active substance release from poly(ethylene oxide) hydrogels. *Int. J. Pharm.* **2001**, *224* (1), 151–158.

(48) Jensen, T.; Kelly, L.; Lazarides, A.; Schatz, G. C. Electrodynamics of Noble Metal Nanoparticles and Nanoparticle Clusters. *J. Cluster Sci.* **1999**, *10* (2), 295–317.

(49) Palik, E. D. *Handbook of Optical Constants of Solids*; Academic Press: New York, 1985.

(50) Landau, L. D.; Lifshitz, E. M. *Electrodynamics of Continuous Media*; Oxford University Press: New York, 1960.

(51) To calculate this value, we first assume that an exciton is localized inside a small cylindrical fraction of NW of length $2R_{NW}$. Then, the total rate of transfer is calculated as a sum: $\gamma_{transfer}(\omega_{exc}) = \sum_i \gamma_{1,transfer}(\omega_{exc},d_i)$, where d_i is the distance between the exciton center and the center of i-Au-NP and i is the Au-NP number.

(52) Lakowicz, J. R. *Principles of Fluorescence Spectroscopy*, 3rd ed.; Plenum Press: New York, 2006.

(53) Fofang, N. T.; Park, T. H.; Neumann, O.; Mirin, N. A.; Nordlander, P.; Halas, N. J. Plexcitonic Nanoparticles: Plasmon−Exciton Coupling in Nanoshell-J-Aggregate Complexes. *Nano Lett.* **2008**, *8* (10), 3481–3487.

(54) Baer, R.; Neuhauser, D.; Weiss, S. Enhanced Absorption Induced by a Metallic Nanoshell. *Nano Lett.* **2003**, *4* (1), 85–88.

JP809780M